THE JOURNAL OF PHYSICAL CHEMISTRY B

Article

pubs.acs.org/JPCB

Exploration of the Pyrazinamide Polymorphism at High Pressure

Xiao Tan,[†] Kai Wang,[†] Shourui Li,[†] Hongsheng Yuan,[†] Tingting Yan,[†] Jing Liu,[‡] Ke Yang,[§] Bingbing Liu,[†] Guangtian Zou,[†] and Bo Zou[†,*]

[†]State Key Laboratory of Superhard Materials, Jilin University, Changchun 130012, China

[‡]Beijing Synchrotron Radiation Laboratory, Institute of High Energy Physics, Chinese Academy of Sciences, Beijing 100039, China

[§]Shanghai Synchrotron Radiation Facilities, Shanghai Institute of Applied Physics, Chinese Academy of Sciences, Shanghai 201204, China

Supporting Information

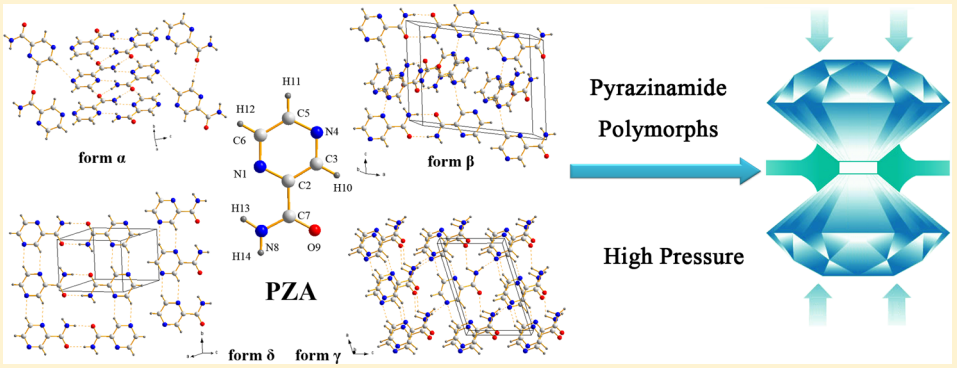

ABSTRACT: We report the high-pressure response of three forms (α, δ, and γ) of pyrazinamide ($C_5H_5N_3O$, PZA) by in situ Raman spectroscopy and synchrotron X-ray diffraction techniques with a pressure of about 14 GPa. These different forms are characterized by various intermolecular bonding schemes. High-pressure experimental results show that the γ phase undergoes phase transition to the β phase at a pressure of about 4 GPa, whereas the other two forms retain their original structures at a high pressure. We propose that the stabilities of the α and δ forms upon compression are due to the special dimer connection that these forms possess. On the other hand, the γ form, which does not have this connection, prefers to transform to the closely related β form when pressure is applied. The detailed mechanism of the phase transition together with the stability of the three polymorphs is discussed by taking molecular stacking into account.

INTRODUCTION

Polymorphism is the ability of a compound to exist in multiple crystalline forms.[1] This ability has attracted considerable attention from chemists, physicists, and pharmacologists.[2−6] Polymorphs with various molecular arrangements can have different physicochemical properties, such as melting point, stability, solubility, and density.[6−8] These properties are particularly important in the pharmaceutical industry especially when practical considerations are taken into account, such as bioavailability, processability, and storage.[6,9] As one of the most important noncovalent interactions, hydrogen bonding possesses the characteristic properties of reversibility, directionality, and saturability.[10,11] It has a crucial function in pharmaceutical applications. Pressure is a powerful tool in controlling the strength and geometric properties of a given D−H···A hydrogen bond (D and A mean donor and acceptor, respectively).[12−14] High-pressure studies of hydrogen-bonded polymorphic compounds can provide more information about the nature of hydrogen bonding.[15] Hydrogen bonding also assists in the investigation of interconversion among different polymorphs and in the generation of new polymorphs, which is a basic issue in supramolecular chemistry and crystal engineering.[7,11,16−20] Furthermore, given the excellent ability of pressure to modify the structures and properties of pharmaceuticals, a pure or new form can be obtained to develop drugs with higher efficacy. Therefore, the study of different polymorphic architectures of pharmaceuticals and hydrogen bonding is of fundamental and practical importance.

In the past decade, organic polymorphic systems including pharmaceuticals, amino acid, and energetic materials, have been extensively studied in high-pressure conditions.[21−28] Two polymorphs of paracetamol were investigated to obtain information about the relevance of hydrogen bonding and crystal structure.[24] Form III of piracetam transforms to form I at a compression of 0.2 GPa at 443 K.[15] Glycine is a textbook example in the high-pressure investigation of polymorphism. The α form of glycine is stable to 23 GPa, the β form undergoes phase transition to a new form at 0.76 GPa, and the

Received: April 23, 2012
Revised: October 31, 2012

   dx.doi.org/10.1021/jp3039219 | J. Phys. Chem. B XXXX, XXX, XXX−XXX

γ phase transforms to ε phase at 2 GPa. These studies suggest that pressure has an unrivalled ability to modify crystal structures, especially in transition among different forms or forming new phases. Moreover, hydrogen-bonded interaction has an important effect on phase transitions at the molecular level.

Pyrazinamide (pyrazine-2-carboxamide, abbreviated as PZA, $C_5H_5N_3O$) is one of the first-line drugs in antituberculosis treatment and is on the WHO Model List of Essential Medicines.[29,30] It is a rare example of a conformationally rigid molecule with four polymorphs, namely α, β, γ, and δ forms.[31−35] The best crystallographic data on the four polymorphs of PZA are summarized in Table 1.[31−35] The intrinsic dissolution rates for the α, δ, and γ forms are 2.07, 2.05, and 2.78 mg cm^{-2} min^{-1}, respectively, with an order of $\delta < \alpha < \gamma$. PZA, a model pharmaceutical system for studying phase relationships among the four polymorphs, has been extensively investigated at ambient pressure. When pure δ and γ forms are subjected to manual grinding, they convert to the α form in 45 min. Upon heating to 165 °C, the α, β, and δ forms transform into the γ form. After cooling to room temperature, the γ form can be stable for up to 6 months but progressively converts to the α form. In other words, a stable form at a high temperature can be retained at ambient temperature as a metastable form. The α form transforms into the δ form in the temperature range −263 to −13 °C. Previous studies that combined semischematic energy-temperature diagram, phase transformation experiments, thermal measurements, and crystal structure data determined the order of the free energy as follows: $\alpha < \delta < \gamma < \beta$ at 25 °C, $\gamma < \alpha < \delta < \beta$ at 160 °C, and $\delta < \alpha < \beta < \gamma$ at absolute zero. Although the δ polymorph has the lowest free energy at absolute zero temperature, the α polymorph is the more relevant form to crystallization and handling of pharmaceuticals under ambient conditions.[36,37]

In the present study, we present high-pressure Raman scattering and in situ synchrotron angle dispersive X-ray diffraction (ADXRD) studies by using a diamond anvil cell (DAC) for three pure forms (α, δ, and γ) of PZA at a pressure of up to 14 GPa. Synchrotron XRD results provide the structural information of the three forms. Raman scattering measurements probe the evolution of different hydrogen-bonded connections. Our primary goal is to find the phase transition among the different polymorphs, and to further provide a better understanding of the stability of the polymorphs.

Table 1. Crystallographic Parameters of PZA Polymorphs (100 K)

polymorph	α form	β form	γ form	δ form
chemical formula	$C_5H_5N_3O$	$C_5H_5N_3O$	$C_5H_5N_3O$	$C_5H_5N_3O$
formula weight	123.12	123.12	123.12	123.12
crystal system	monoclinic	monoclinic	monoclinic	triclinic
space group	$P2_1/n$	$P2_1/n$	Pc	$P\bar{1}$
a/Å	3.6147(4)	14.315(2)	7.1756(14)	5.1186(10)
b/Å	6.7384(8)	3.6238(5)	3.6508(7)	5.7053(11)
c/Å	22.464(3)	10.6158(15)	10.663(2)	9.857(2)
α/deg	90	90	90	97.46(3)
β/deg	92.499(2)	101.119(2)	106.337(3)	98.17(3)
γ/deg	90	90	90	106.47(3)
Z	4	4	2	2
V/Å^3	546.63(11)	540.34(13)	268.05(9)	268.82(9)
CCDC no.	PYRZIN15	771182	PYRZIN17	PYRZIN16

EXPERIMENTAL SECTION

The commercially available α form of PZA (Sigma-Aldrich) was used as the source material in all of our experiments. Further purification of α-PZA was performed by recrystallization from water. The δ form was obtained from toluene. The original material (0.05 mmol) was dissolved in 6 mL of the solvent and

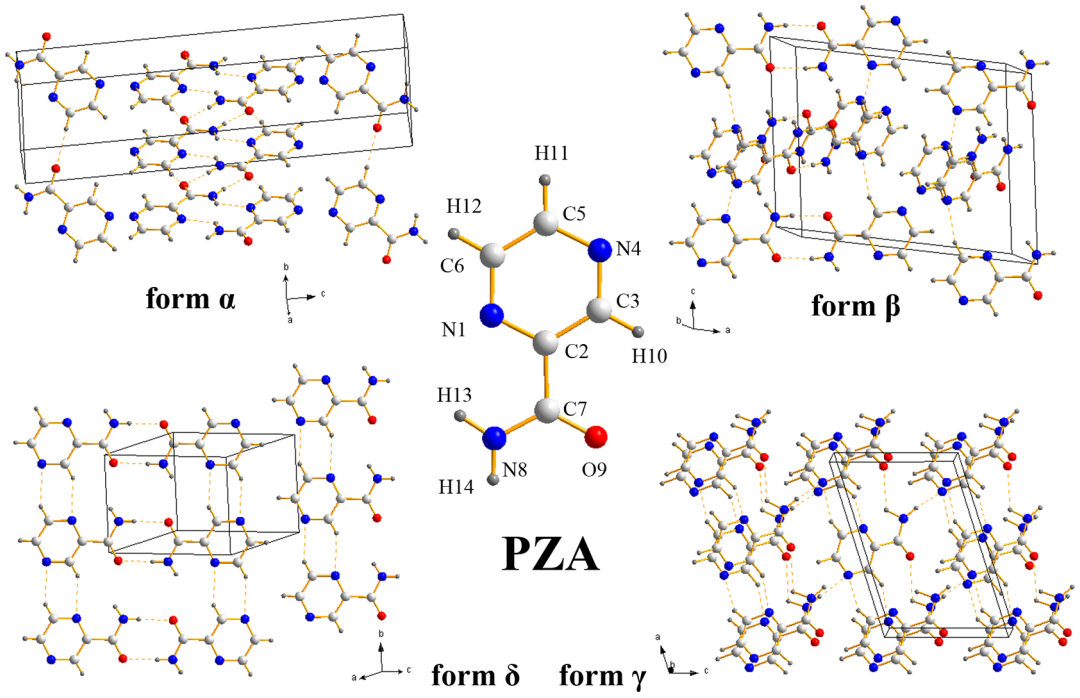

Figure 1. Crystal structures of PZA polymorphic forms: α, β, δ, and γ forms.

dx.doi.org/10.1021/jp3039219 | J. Phys. Chem. B XXXX, XXX, XXX−XXX

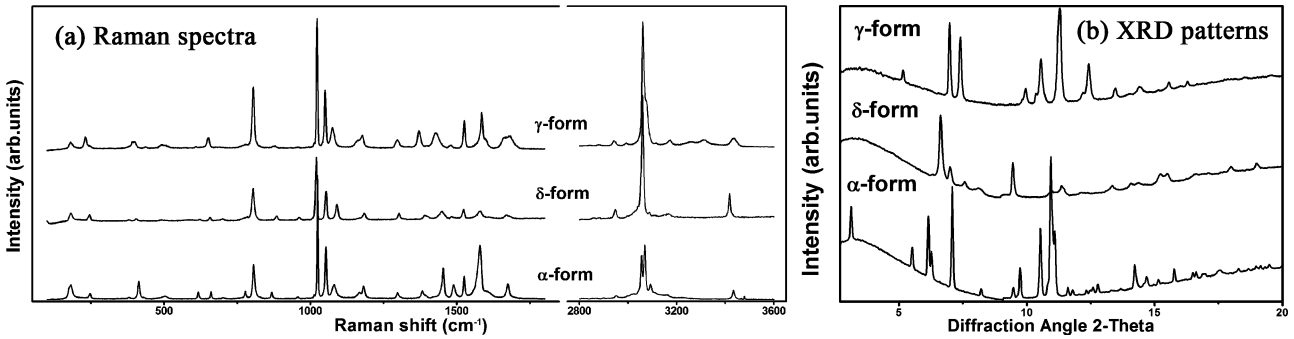

Figure 2. Raman spectra (at ambient condition) and XRD patterns (in DAC) of the three polymorphs.

left to evaporate slowly at room temperature.[36] The γ form was obtained by heating the α form for 90 min at 140 °C. The purity of the α, δ, and γ polymorphs were confirmed by XRD patterns. Flawless crystals were selected and gently ground for 20 min to obtain powders with a size of approximately several micrometers. These powders were used for the high-pressure Raman and synchrotron experiments. The powder samples were used for Raman measurements to address the effect of orientation in single crystals and to remain consistent with synchrotron experiments.

High-pressure experiments were carried out using DAC. The culet diameter of the diamond anvils was 0.5 mm. T301 stainless steel gaskets were preindented to a thickness of 60 μm, and center holes of 0.16 mm were drilled for the sample. The ruby chip was used for pressure determination using the standard ruby fluorescent technique.[38] A 4:1 mixture of methanol and ethanol was used as the pressure-transmitting medium. All experiments were performed at room temperature.

Raman scattering measurements were conducted using two laser wavelengths as the excitation. An argon ion laser (514.5 nm) was used in the region 100−3600 cm^{-1} for the γ form using a Jobin Yvon HR800 microspectrometer. The 830 nm line from a near-infrared diode laser of a Renishaw inVia Raman system was used in the range 300−2000 cm^{-1} for the α and δ forms to avoid a strong fluorescence signal. The resolution of the Raman system was 1 cm^{-1} and integration time was 30 s.

In situ ADXRD experiments were performed at the 4H2 High-Pressure Station of Beijing Synchrotron Radiation Facility. A 0.6199 Å beam with a spot size of 20 × 30 μm^2 was used as the incidence light source. Portions of this work were performed using the BL15U1 beamline at the Shanghai Synchrotron Radiation Facility, where a monochromatic 0.6199 Å radiation with a spot size of 5 × 5 μm^2 was used for data collection. Typical Bragg rings were recorded with an image-plate area detector (Mar 345). An average acquisition time of 300 s was adopted for each pattern, considering the small cross sections for light atoms (C, H, O, and N) in PZA. Two-dimensional data were obtained and converted to plots of intensity versus 2θ by using the Fit2D software.[39] Further analysis of the XRD patterns were performed using the Materials Studio program 5.0 (Accelrys Inc.).

RESULTS AND DISCUSSION

The molecule packing in different polymorphs is shown in Figure 1. In the α polymorph, the molecules are linked in centrosymmetric planar dimers by $N_8-H_{14}\cdots O_9$ that aggregate sideway with other dimers, thereby forming planar ribbons with $C_6-H_{12}\cdots O_9$ and $N_8-H_{13}\cdots N_1$. Neighboring ribbons are joined by $C_5-H_{11}\cdots N_4$ interactions, but the ribbons do not share the same plane. In the β polymorph, a similar formation of centrosymmetric planar dimers that aggregate sideways with other dimers through $C_3-H_{10}\cdots N_1$ and $C_6-H_{12}\cdots N_4$ was observed. The planes of consecutive dimers form an angle of 49.5° to allow a closer arrangement of the dimers. In the δ polymorph, the molecules are linked in pairs with the same head-to-head dimerization. The dimers aggregate sideways with others and form planar chains through $C_3-H_{10}\cdots N_1$ interactions. The chains assemble in layers. Compared with the three forms above, the molecules of the γ polymorph assemble head-to-tail with each molecule and form an angle of 49.3° with its closest neighbors by $N_8-H_{14}\cdots N_4$ interactions. The molecular chains form a 3-D structure with $N_8-H_{13}\cdots O_9$, $C_6-H_{12}\cdots N_4$ and $C_3-H_{10}\cdots O_9$ on the side with no dimers. The hydrogen bonds mentioned above are all intermolecular connections. The primary connections of the four forms (dimerization in α, β, and δ, head-to-tail aggregation in γ) are presented in Figure 1. Figure 2 shows the powder XRD patterns in the DAC and the Raman spectra at ambient condition of the three polymorphs. The Raman spectrum of the α form is in agreement with those reported in the literature.[36,37,40] Table 2 summarizes the assignments of the Raman modes of different polymorphs, and the indices of the atoms are consistent with the numbers of PZA molecule in Figure 1.

Compression Study of α-PZA. The evolution of Raman spectra for α phase as a function of pressure is depicted in Figure 3. The sharp Raman line at 1332 cm^{-1} is a signature of diamond. Apart from the C−H in-plane bending at about 1300 cm^{-1}, all Raman modes show expected blue shifts. This shift is due to the decrease in interatomic distances and the increase in effective force constants with increasing pressure. The mode assigned to ring-bending at ∼415 cm^{-1} broadens at the lowest pressure. Splitting, which is marked by an arrow in Figure 3, can be seen clearly at 4.3 GPa. The splitting of this mode indicates the deformation of the ring with increasing pressure. The C−H in-plane bending mode exhibits red shifts throughout the experimental process. A previous study reported that increasing the pressure would decrease the D−H bending frequencies and increase the D−H stretching frequencies of strong hydrogen bonds.[41] The blue shift of the C−H stretching mode (see Figure S1, Supporting Information) and the red shift of the C−H in-plane bending mode indicate that the hydrogen bond becomes stronger with increasing pressure. The Raman profiles suggest that the structure remains unchanged upon compression. The frequency shifts and the rates of shifting of the Raman features with increasing pressure are presented in Figure S2 and in Table S1 (Supporting Information), respectively.

dx.doi.org/10.1021/jp3039219 | J. Phys. Chem. B XXXX, XXX, XXX−XXX

Table 2. Tentative Assignment for Raman Bands of Three Pyrazinamide Polymorphs[a]

assignment	frequencies (cm^{-1}) form α	form δ	form γ
$\upsilon_{as}(NH_2)$	3430	3424	3433
$\upsilon_{s}(NH_2)$			3313
$\upsilon_{s}(NH_2)$ HB			3256
$\upsilon_{s}(NH_2)$ HB	3155		3172
$\upsilon(C_3H)$	3089		
$\upsilon(C_5H) + \upsilon(C_6H)$	3066	3065	3076
$\upsilon(C_5H) - \upsilon(C_6H)$	3051	3057	3061
combination band	3039		2938
	3012		2892
	2950	2948	2838
$\upsilon(CO) + \delta(NH_2)$	1673	1671	1678
$\upsilon(C_2C_3) + \upsilon(C_5C_6) + \delta(NH_2)$	1578	1583	1585
$\upsilon(N_1C_2) + \upsilon(N_4C_5) - \upsilon(N_1C_6) - \upsilon(N_3C_4)$	1525	1528	1525
$\upsilon(N_1C_2) - \upsilon(N_4C_5) + \delta(C_6H) - \delta(C_3H) + \delta(C_5H)$	1488	1481	1479
$\upsilon(C_2C_7) - \upsilon(C_7N_8) + \delta(C_5H) + \delta(N_8H_{14})$	1452	1443	1429
$\upsilon(C_2C_3) - \upsilon(C_5C_6) + \delta(C_5H) + \delta(C_3H) + \delta(NH_2)$	1382	1391	1370
$\delta(C_3H) + \delta(C_6H)$	1297	1314	1398
$\upsilon(N_1C_6) + \upsilon(N_4C_5) - \upsilon(C_2C_3) - \upsilon(C_5C_6) + \rho(NH_2)$	1181	1182	1177
$\delta(C_5H) - \delta(C_3H)$	1168	1169	1161
$\rho(NH_2)$	1080	1095	1075
$\delta(C_3N_4C_5) + \delta(C_3H)$	1053	1049	1050
$\delta(C_2N_1C_6) - \delta(C_3N_4C_5)$	1024	1021	1023
$\gamma(C_6H) - \gamma(C_3H) - \gamma(C_5H)$	957	959	
$\tau(NH_2)$	868	866	875
$\delta(N_1C_2C_3) + \delta(N_4C_5C_6) + \rho(NH_2)$	807	805	805
$\gamma(N_1C_2) + \gamma(C_7C_2) + \gamma(C_5C_6) + \gamma(C_3H) + \gamma(C_5H)$	777	784	778
δ(ring)	661	653	651
$\tau(NH_2)$	618	608	607
$\rho(NH_2) + \delta(C_2C_7N_8) + \rho$(ring)	504	505	497
$\gamma(N_1C_2) + \gamma(N_4C_5) - \gamma(C_7O_9)$	415	410	435
$\gamma(C_2C_3) + \gamma(C_6N_1) + \gamma(N_4C_3)$	382	384	396
ρ(ring)	248	247	230
lattice modes	178	180	180
	117	140	118
		123	104

[a] υ, stretching; γ, out-of-plane bending; τ, twisting; ρ, rocking; δ, in-plane bending and HB, hydrogen bonded; s, symmetric; as, asymmetric.

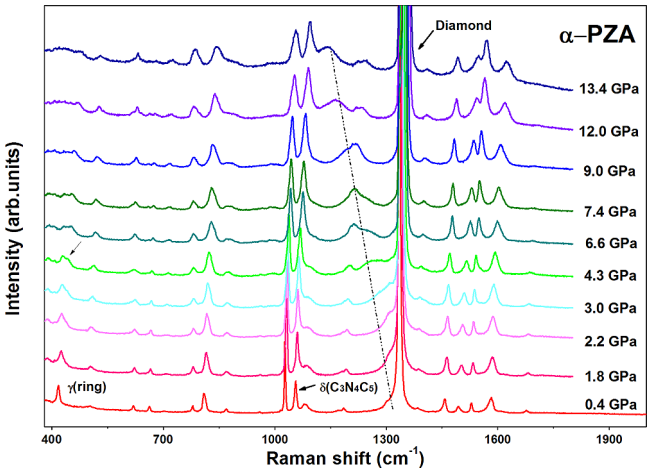

Figure 3. Evolution of Raman spectra of the α form at high pressures in the range 300−1800 cm^{-1}.

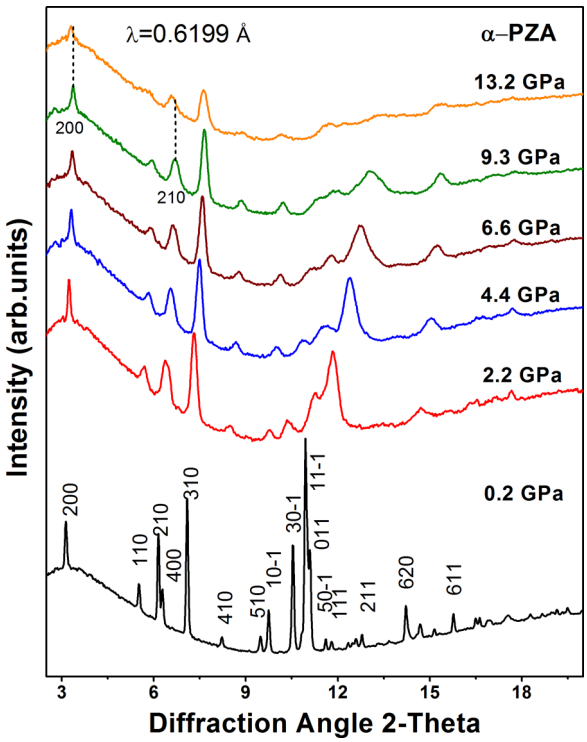

Figure 4. Representative ADXRD patterns of the α phase at different pressures. Dashed lines are given for the sake of clarity of two peaks shifting to lower angles.

Representative XRD patterns of α phase at various pressures are shown in Figure 4. No discernible phase transitions can be observed according to the XRD patterns. The pressure evolutions of the unit cell volume and the lattice parameters are illustrated in Figure S3 (Supporting Information). The curve of the relative unit-cell volume versus pressure is fitted to a two-parameter Murnaghan equation of state (MEOS):

$$P = \frac{B_0}{B_0'}\left[\left(\frac{V_0}{V}\right)^{B_0'} - 1\right]$$

where B_0 and B_0' are the ambient bulk modulus and its pressure derivative, respectively,[42] and V_0 is fixed as the value at ambient conditions ($V_{0\alpha}$ = 577.773 Å^3, $V_{0\beta}$ = 559.730 Å^3, $V_{0\delta}$ = 279.557 Å^3, and $V_{0\gamma}$ = 275.136 Å^3). The best fits are B_0 = 3.8 ± 0.5 GPa and B_0' = 8.4 ± 0.9. The effect on the lattice constants at a high pressure is anisotropic. From an ambient pressure to 9.3 GPa, the *a*-axis is reduced by 5%, the *c*-axis by 20%, and the *b*-axis by 13%. In Figure 4, the peaks (200) and (210) progressively shift to a low-angle after 9.3 GPa. This indicates that the *a*-axis expands upon further compression. The expansion, which is caused by the change in angles between the adjacent molecules, is similar to a phenomenon observed in paracetamol.[24] This expansion results from the cooperative rotations of molecules within the layer and the flattening of the layers, accompanied by a shortening of the intermolecular hydrogen bonds.[24] The intensity of all diffraction peaks is much smaller at 13.2 GPa than at 9.3 GPa. This result indicates the beginning of amorphization. When the pressure is above 10 GPa, the increased energy of intermolecular interactions rotate mole-

dx.doi.org/10.1021/jp3039219 | J. Phys. Chem. B XXXX, XXX, XXX−XXX

cules and distort the hydrogen bond networks, then the amorphization takes place to achieve closer packing with an effort to reduce the free energy.[11] In conclusion, α-PZA is stable in the pressure range 0−13 GPa in accordance with the results of Raman spectra.

Compression Study of δ-PZA. The Raman spectra obtained at various pressures in the δ phase are shown in Figure 5. No significant change in the Raman profiles is

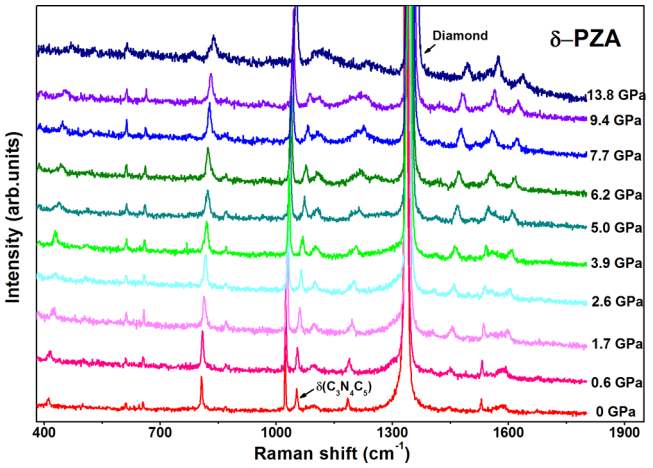

Figure 5. Evolution of Raman spectra of the δ form at high pressures in the range 380−800 cm^{-1}.

observed with increasing pressure. Figure S5 shows the pressure-induced shifts of these observed Raman modes (see Supporting Information). No discontinuities of the Raman modes with increasing pressure are detected. Thus, we can conclude that the structure of the δ phase is stable up to ~13 GPa. The two Raman modes in the range 1000−1150 cm^{-1} of δ phase have the same assignment as in the α phase but with different pressure dependence. The intensity of the peak at 1053 cm^{-1} ($\delta(C_3N_4C_5)$) for the α phase is enhanced with increasing pressure, whereas the peak at 1049 cm^{-1} assigned to the same Raman mode for the δ phase decreases in intensity and broadens in peak width. We propose that the different surrounding environments of the ring group is responsible for the different evolution.[43] The pyrazine ring in the α phase is linked with the corresponding amino group by N−H···N hydrogen bonds that do not exist in the δ phase. Furthermore, the diversity in the topographical nature of the layers may also contribute to the differences in the relative intensities between the two phases. A similar phenomenon is observed in the range 700−800 cm^{-1} for the same reason.

The evolution of XRD patterns versus pressure for the δ phase is illustrated in Figure 6, where all peaks shift to higher diffraction angles with different rates because of the decrease in interatomic distances. No discernible phase transition can be observed up to 13 GPa. The calculated values of bulk modulus and its pressure derivative for MEOS are B_0 = 9.2 ± 0.8 GPa and B_0' = 9.5 ± 0.9 respectively (see Supporting Information). Moreover, the response to pressure is anisotropic, but no expansion takes place in the δ phase. Compared with the α phase in which the dimers do not share the same plane in monoclinic structure, the layers in the δ phase are already flat at ambient pressure. The ADXRD results are consistent with conclusion from the Raman measurements that the crystal retains its original symmetry up to ~13 GPa.

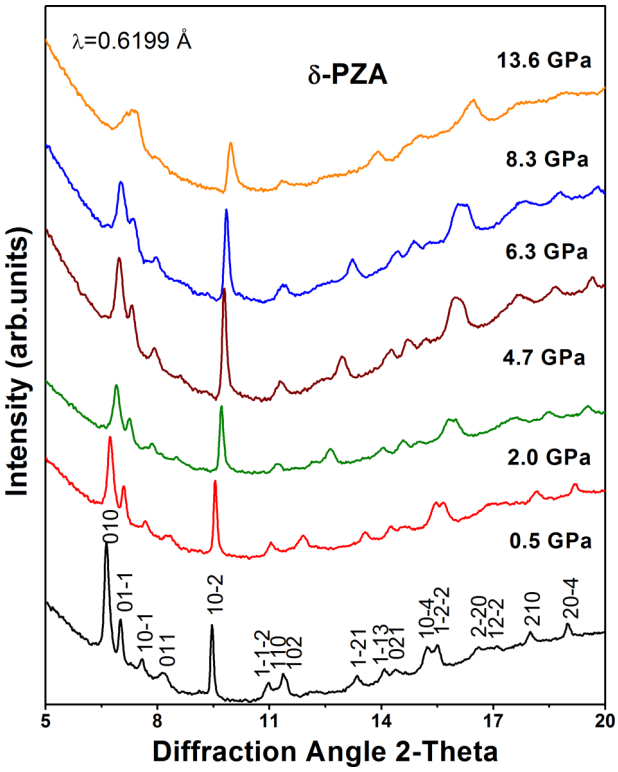

Figure 6. Representative ADXRD patterns of the δ phase at high pressures.

Compression Study of γ-PZA. The evolution of Raman spectra ranging from 80 to 350 cm^{-1} at different pressures is shown in Figure 7. The spectrum at ambient conditions consists of three lattice modes and an internal mode of ρ(ring) marked by arrows in the figure. The three lattice modes show

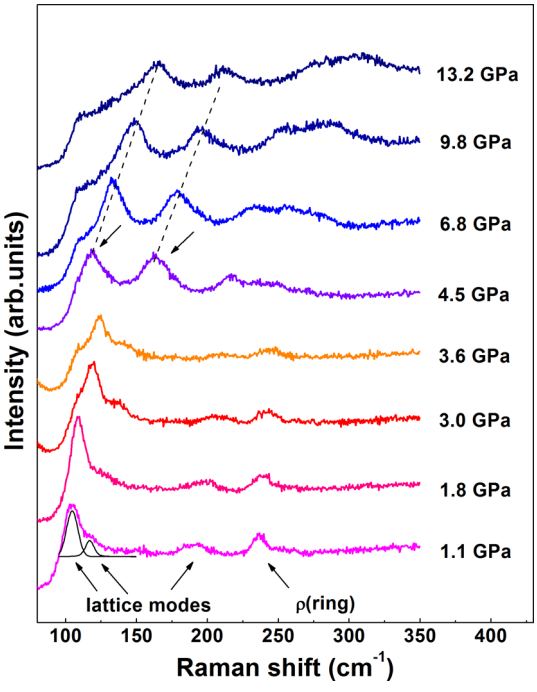

Figure 7. Representative Raman spectra of the γ form between 80 and 350 cm^{-1} at various pressures. The dotted lines are used to indicate the lattice modes' evolution.

dx.doi.org/10.1021/jp3039219 | J. Phys. Chem. B XXXX, XXX, XXX−XXX

substantial blue shifts with increasing pressure and are sensitive to subtle changes in pressure because of weak noncovalent interactions. Upon further compression, the lattice modes exhibit obvious changes at 4.5 GPa, which indicates the onset of a phase transition. We consider the phase transition to be reconstructive because the spectra at 3.6 and 4.5 GPa are essentially different. The new spectrum gradually shifts to higher wavenumbers without any discontinuity upon compression to 13 GPa, which is the highest pressure used in this experiment. As seen in Figure 8, the pressure dependence of

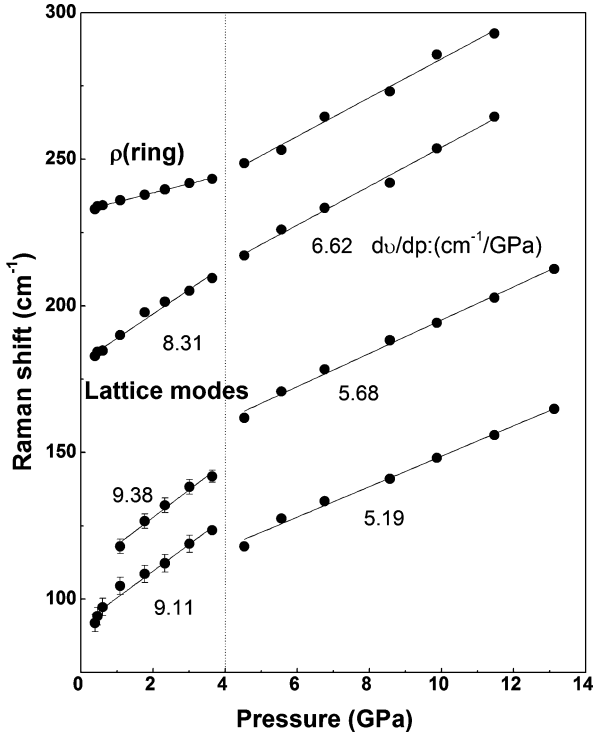

Figure 8. Pressure dependence of the four modes in the range 80−350 cm^{-1} of the γ form. Linear fits are performed for clarity. The dotted line represents the boundary of the two phases.

the lattice modes shows an obvious discontinuity of slope at ∼4 GPa. This behavior is consistent with the aforementioned phase transition. The linear pressure coefficients of lattice modes in the high-pressure phase are much smaller than those in the original γ phase, which suggests that the new phase adopts a more efficient crystal packing.

The high-pressure Raman spectra of γ-PZA in the range 350−1800 cm^{-1} and the pressure dependence of these modes are depicted in Figures 9 and 10, respectively. From an ambient pressure to 3.6 GPa, all observed internal modes display normal blue shifts. Nevertheless, several significant changes in this range are observed across 4.5 GPa: the splitting of the ring out-of-plane bending mode γ(ring), red shift of the ring in-plane bending mode δ(ring), and the emergence of new modes. These changes also suggest a phase transition at this pressure. In detail, the mode at 807 cm^{-1} assigned to the δ(ring) broadens and abruptly displays a red shift, which indicates that the pyrazine ring undergoes significant modifications from 3.6 to 4.5 GPa. Two new Raman modes, marked with exclamation symbols, appear with a pronounced intensity at 4.5 GPa and become dominant upon further compression, whereas the modes from the original γ phase decreases and eventually vanishes at pressures above ∼9 GPa. The discontinuity of these Raman modes with increasing pressure in the range 3.6−4.5 GPa can be clearly observed in Figure 10. The size and direction ("blue" or "red") of the frequency jumps are different for each bond, which implies the change in the environment around the atoms or the functional groups through the phase transition.

In Figure 11, we present the typical Raman spectra of the C−H and N−H stretching modes at various pressures. As shown in Figure 11a, the two C−H stretching modes (3061 and 3076 cm^{-1}) reveal blue shifts because of the repulsive nature of the chemical environment around them up to 3.6 GPa. However, the N−H stretching modes display different high-pressure behaviors (red or blue shift) because of the variation in strength of the hydrogen bonds.[44] The red shift can be attributed to the corresponding weak hydrogen bonds, of which the strength can be enhanced with increasing pressure.[44] In weak and moderate hydrogen bonds, pressure can shorten the distance between D and A, followed by contraction of the H···A distance because of the increasing electrostatic attraction between H and A. The subsequent extension of the D−H distance results in a red shift of the D−H stretching modes, whereas the blue shift can be traced to strong hydrogen bonds because of the continuous enhancement of hydrogen bonds at high pressure.[41,44] A considerable redistribution of intensities and positions is observed at 4.5 GPa. In other words, the position and/or orientation of the molecules has changed, which provokes a modification of the bonding scheme. When the pressure was further increased, the modes gradually lose their intensities and fade into the background. The pressure dependence of the selected stretching modes is shown in Figure 11b. An obvious discontinuity exists in the range 3.6−4.5 GPa, which demonstrates the reconstructive nature of the hydrogen bonds through the phase transition. Above 4.5 GPa, new stretching modes exhibit red or blue shifts because of the different strengths of the hydrogen bonds. From the Raman results, a pressure-induced phase transition occurs at 4.5 GPa.

We performed high-pressure XRD measurements to demonstrate further the pressure-driven phase transition in γ-PZA. These measurements can provide straightforward evidence for the existence of phase transition. The evolution of the XRD patterns during compression and decompression is illustrated in Figure 12. As shown in the figure, all peaks shift to high diffraction angles with increasing pressure below 4 GPa because of the decrease in interatomic distances. Meanwhile, γ-PZA exhibits a high and anisotropic compressibility. However, two new diffraction peaks emerge and are marked by the arrows at ∼4 GPa. The emergence of these peaks indicates the onset of a phase transition. From 4 to 8 GPa, the diffraction patterns clearly show the coexistence of the original and the high-pressure phases, which is consistent with the evolution observed in the Raman spectra. The high-pressure phase retains its stability up to 14 GPa. When the pressure was released, the γ form is not detected until the pressure was released to ambient, as can be clearly seen in Figure 13 (upper panel). The phase transition is reversible with an obvious hysteresis (approximately 4 GPa). However, what is the structure of the high-pressure phase? Is it possibly the known polymorph? With these questions in mind, we carefully examine the structures of the other polymorphs. Based on the comparison, the experimental XRD profiles from the high-pressure phase (13.2 GPa↑ and 0.7 GPa↓) are quite similar to the simulated pattern of the pure β polymorph. Thus, we

dx.doi.org/10.1021/jp3039219 | J. Phys. Chem. B XXXX, XXX, XXX−XXX

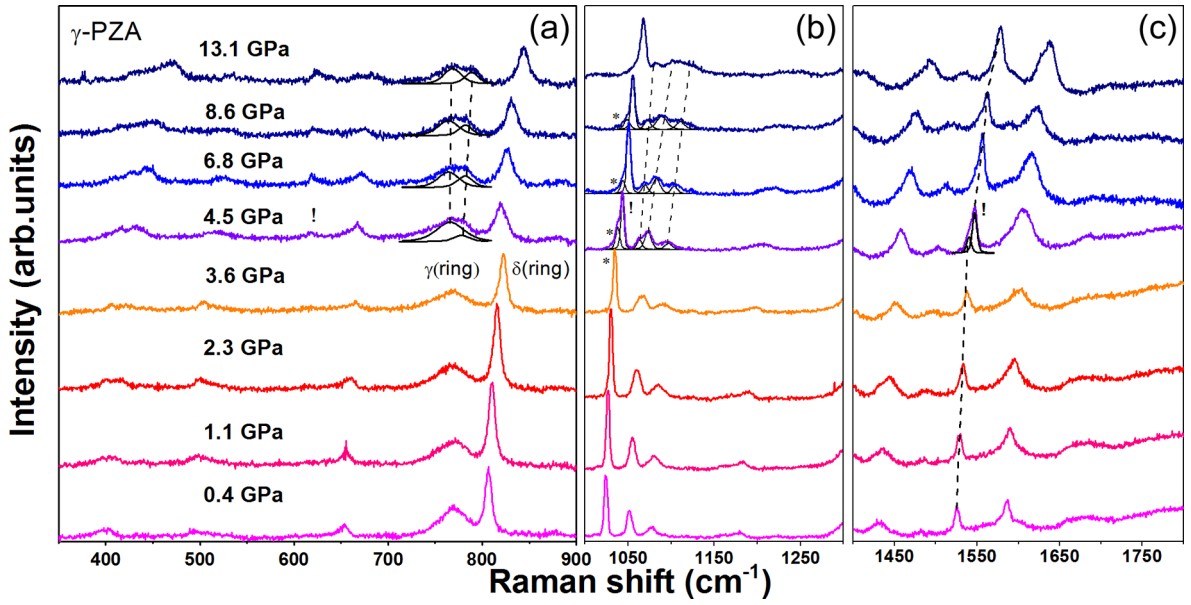

Figure 9. Evolution of Raman spectra of the γ form at high pressures in the following ranges: (a) 300−900 cm^{-1}; (b) 1000−1300 cm^{-1}; (c) 1400−1800 cm^{-1}. Decomposition of the spectra and dashed lines are performed for clarity. Asterisks denote the original peaks of the γ form, and the exclamation marks denote the additional peaks appearing above 4 GPa.

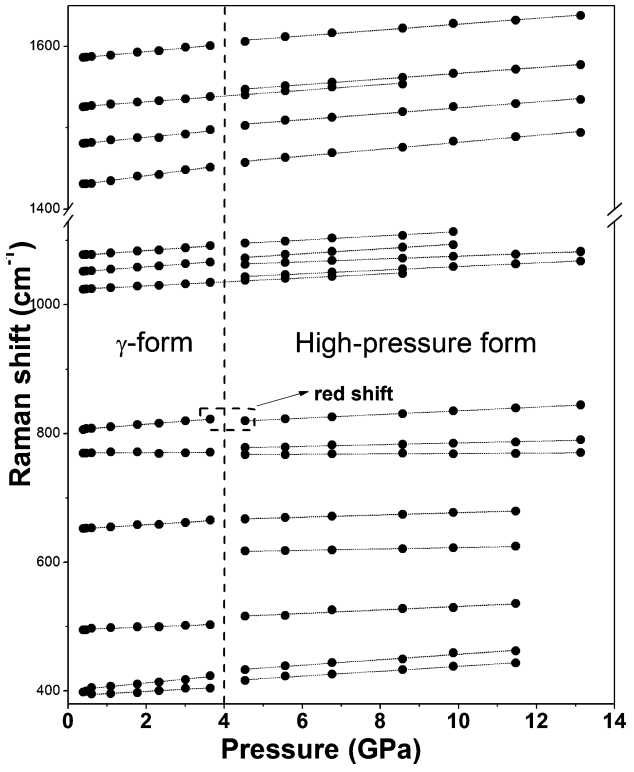

Figure 10. Frequency shifts of major internal modes ranging from 380 to 1700 cm^{-1} as a function of pressure. The vertical dotted lines represent the boundary of the two phases.

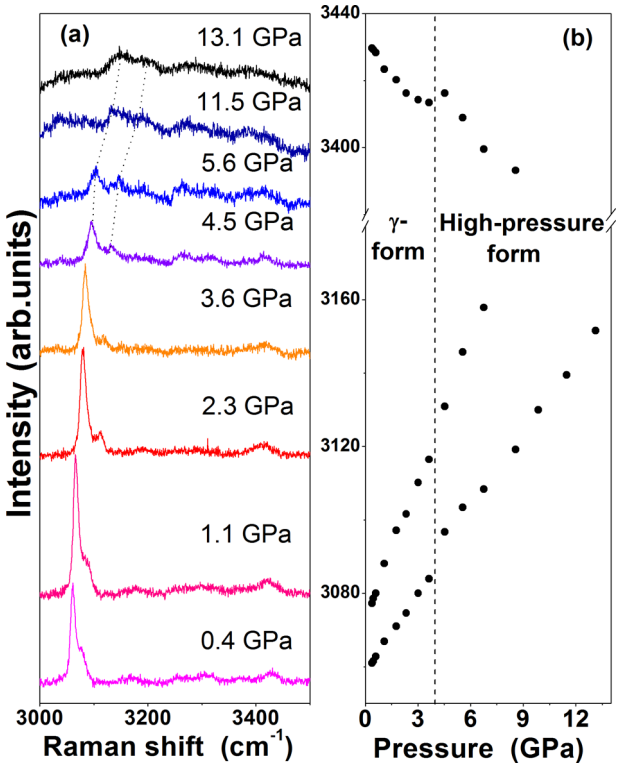

Figure 11. (a) Evolution of Raman spectra of the γ form in the range 3000−3600 cm^{-1} at selected pressures. (b) Frequency shifts of the selected modes in this range as a function of pressure. The vertical line represents the boundaries of the different phases.

suspect that the high-pressure phase might be the β phase. We then simulated the diffraction pattern at 0.7 GPa of the β form based on the ambient structure. The intuitive comparison is presented in Figure 13 (lower panel), and the result confirms our speculation. The crystal symmetry changes from *Pc* to $P2_1/c$, and the lattice parameters are a = 14.20(3) Å, b = 3.43(2) Å, c = 10.26(6) Å, β = 101.12(2)°, and V = 491.04(9) $Å^3$ at 0.7 GPa. The pressure dependence of the lattice constants and unit cell volume are illustrated in Figure 14. The volume is reduced by ∼3% at pressure greater than 4 GPa, and the bulk modulus and its pressure derivatives for the γ and β forms are shown as follows:

γ form: B_0 = 6.3 ± 0.4 GPa, B_0' = 10.0 ± 0.3

dx.doi.org/10.1021/jp3039219 | J. Phys. Chem. B XXXX, XXX, XXX−XXX

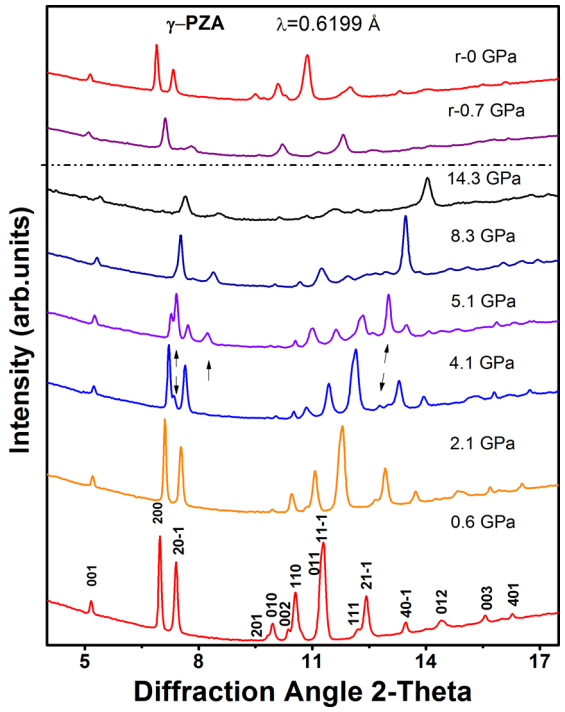

Figure 12. Representative XRD patterns of the γ phase at high pressures. The wavelength for data collection is 0.6199 Å. The upper pattern indicates that the phase transition of the γ phase is reversible.

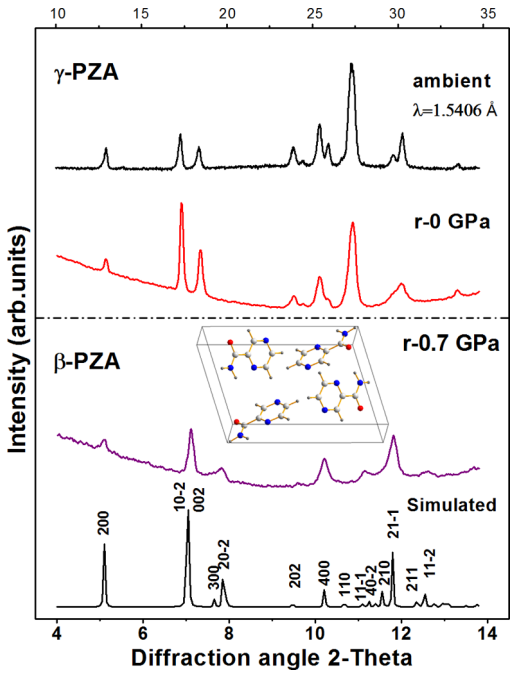

Figure 13. Upper panel: comparison of XRD pattern released from 13 GPa and the one at ambient pressure of the γ form (λ = 1.5406 Å). Lower panel: comparison of XRD pattern released to 0.7 GPa with the simulated pattern at the same pressure for the β form.

$$\beta \text{ form: } B_0 = 7.9 \pm 0.3 \text{ GPa}, B_0' = 5.8 \pm 0.2$$

These equations indicate that the β form is more difficult to compress, which is consistent with the conclusion of lattice vibration analysis in the Raman spectra.

This phase transition sequence is unusual, because the transition occurs between two known polymorphs, and is

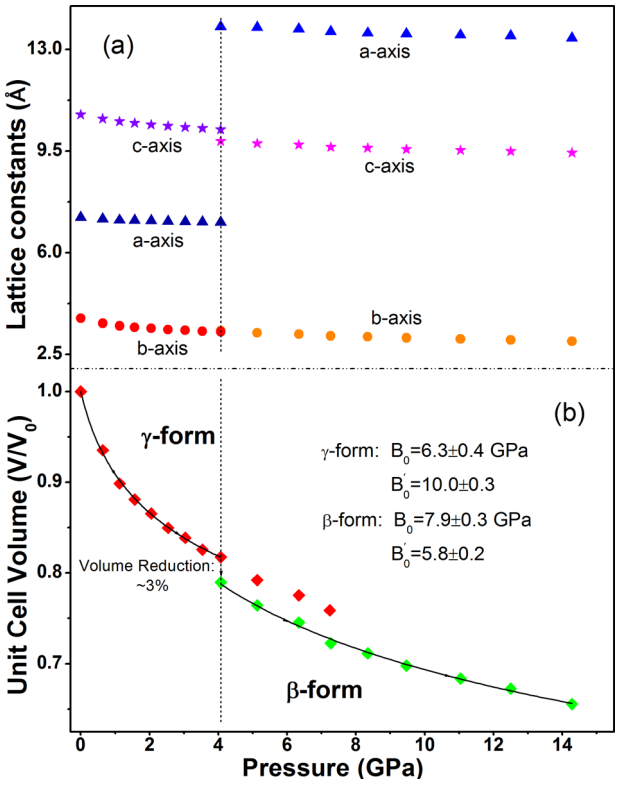

Figure 14. Compression of (a) lattice constants and (b) unit cell volume of the γ and β forms with respect to pressure. The vertical dotted lines represent the boundary of the two phases.

reversible. The transition of form I of resorcinol is also similar.[45,46] The pressure-induced γ-to-β phase transition is observed within a wide pressure range. The hysteresis behavior is very common in high-pressure investigations and is a characteristic of first-order phase transitions. The γ form is not recovered until the pressure is near ambient, which indicates an energy barrier to the transition.[47] To the best of our knowledge, the β form cannot be completely obtained at natural conditions. The β form always crystallizes together with the γ form, which is the third sample in our high-pressure experiment. The free energies of the two forms are quite close to each other with $\gamma < \beta$ at ambient condition. This is consistent with the behavior of the sample releasing to the γ phase and further indicates that the β form is the least stable form at ambient conditions. The predominant intermolecular interactions within γ-PZA are hydrogen bonding and van der Waals interactions. The phase transition can be interpreted by the disturbed balance of these two factors. The distances between PZA molecules within the 3D structure decrease with increasing pressure, which strengths the hydrogen bonding and increases the total Gibbs free energy. Upon further compression, the γ-PZA crystal cannot support the increasing Gibbs free energy any longer. Thus the rotation of the PZA molecules and the reconstruction of hydrogen bonds reduce the free energy, which result in the phase transition at ~4 GPa. The proposed mechanism for the phase transition is consistent with both Raman and ADXRD data.

A discussion on the different high-pressure behaviors of three forms of PZA is of significant interest. The high-pressure results in this study reveal that the α and δ forms retain their original structures at all pressures in the experiments. On the other hand, the γ-to-β phase transition occurs in the γ phase when the

dx.doi.org/10.1021/jp3039219 | J. Phys. Chem. B XXXX, XXX, XXX–XXX

pressure is applied, and the high-pressure β form is stable up to 14 GPa. Previous studies have shown that the dimer connected by relatively strong N−H···O hydrogen bonds is present in the α, β, and δ forms, whereas a head-to-tail connection is present only in the γ form through N−H···N hydrogen bonds.[36,37] On the basis of this fact and on our high-pressure results, we propose that the centrosymmetric dimer structure in the α, β, and δ forms is responsible for their high stability upon compression (14 GPa in our experiments). By comparison, increasing repulsive and steric stresses induced by pressure can be accommodated by the reconstruction of hydrogen bonds in the γ form. Hence, the closely related β form is adopted in γ-PZA at high pressure, where the formation of dimer connection improves its stability. When the pressure was released, the β form reverts to the γ form because the dimer structure in the β form is not as stable as those in the α and δ forms at ambient condition.

CONCLUSION

We performed a combined high-pressure Raman and synchrotron XRD study for the three forms (α, δ, and γ) of PZA up to ∼14 GPa. The phase transition from the γ to the β form at 4 GPa is indicated by both Raman spectra and XRD patterns. The phase transition is associated with the rearrangement of hydrogen bonds caused by competing interactions between hydrogen bonds and the van der Waals force at a high pressure. Moreover, the high-pressure β form remains stable up to ∼14 GPa. This work complements the studies on the relative stability of the PZA polymorphs. This study provides insights for understanding the behaviors of different polymorphs under thermodynamic conditions, which is important for the pharmaceutical industry and for exploring new drugs. Furthermore, this study offers a basis for the consideration of storage, manufacturing process, and selection of polymorphs in the pharmaceutical industry.

ASSOCIATED CONTENT

Supporting Information

Pressure dependence of Raman shifts of PZA polymorphs (Table S1). Raman spectra of α and δ forms at different pressures in the range 2900−3600 cm^{-1} (Figures S1 and S4). Frequency shifts of major Raman modes of α and δ forms ranging from 250 to 3500 cm^{-1} as a function of pressure (Figures S2 and S5). The unit cell volumes of α and δ forms of pressure, and anisotropic pressure response of the reduced lattices constants (Figures S3 and S6). This information is available free of charge via the Internet at http://pubs.acs.org.

AUTHOR INFORMATION

Corresponding Author

*E-mail: zoubo@jlu.edu.cn.

Notes

The authors declare no competing financial interest.

ACKNOWLEDGMENTS

This work is supported by NSFC (Nos. 21073071, 91227202 and 51025206), the National Basic Research Program of China (No. 2011CB808200), Changjiang Scholar and Innovative Research Team in University (No. IRT1132) and the Graduate Innovation Fund of Jilin University (No. 20121041). This work was performed at 4W2 HP-Station, Beijing Synchrotron Radiation Facility (BSRF) which is supported by Chinese Academy of Sciences (Grant No. KJCX2-SW-N20, KJCX2-SW-N03). Portions of this work were performed on the BL15U1 beamline at the Shanghai Synchrotron Radiation Facility (SSRF). Thanks to Dr. Keh-Jim Dunn for his contribution in the English language to this paper.

REFERENCES

(1) McCrone, W.; Fox, D.; Labes, M.; Weissberger, A. *Physics and Chemistry of the Organic Solid State*; Wiley Interscience, 1965, 725.
(2) Bernstein, J. *Cryst. Growth Des.* **2011**, *11*, 632.
(3) Kitamura, M. *J. Cryst. Growth* **2002**, *237*, 2205.
(4) Moulton, B.; Zaworotko, M. *Chem. Rev.* **2001**, *101*, 1629.
(5) Brittain, H. *J. Pharm. Sci.* **2012**, *102* (2), 464.
(6) Bernstein, J. *Polymorphism in molecular crystals*; Oxford University Press: Oxford, U.K., 2002.
(7) Johnstone, R.; Lennie, A.; Parker, S.; Parsons, S.; Pidcock, E.; Richardson, P.; Warren, J.; Wood, P. *Cryst. Eng. Commun.* **2010**, *12*, 1065.
(8) Haleblian, J.; McCrone, W. *J. Pharm. Sci.* **1969**, *58*, 911.
(9) Fabbiani, F.; Pulham, C. *Chem. Soc. Rev.* **2006**, *35*, 932.
(10) Braga, D.; Grepioni, F. *Acc. Chem. Res.* **2000**, *33*, 601.
(11) Wang, K.; Duan, D.; Wang, R.; Lin, A.; Cui, Q.; Liu, B.; Cui, T.; Zou, B.; Zhang, X.; Hu, J.; Zou, G.; Mao, H. *Langmuir* **2009**, *25*, 4787.
(12) Boldyreva, E. *Cryst. Growth Des.* **2007**, *7*, 1662.
(13) Orgzall, I.; Emmerling, F.; Schulz, B.; Franco, O. *J. Phys.: Condens. Matter* **2007**, *20*, 29.
(14) Katrusiak, A.; Szafranski, M.; Podsiadlo, M. *Chem. Commun.* **2011**, *47*, 2107.
(15) Lamelas, F.; Dreger, Z.; Gupta, Y. *J. Phys. Chem. B* **2005**, *109*, 8206.
(16) Fabbiani, F.; Allan, D.; Parsons, S.; Pulham, C. *Cryst. Eng. Commun.* **2005**, *7*, 179.
(17) Li, S.; Li, Q.; Wang, K.; Tan, X.; Zhou, M.; Li, B.; Zou, G.; Zou, B. *J. Phys. Chem. B* **2011**, *115*, 11816.
(18) Li, S.; Wang, K.; Zhou, M.; Li, Q.; Liu, B.; Zou, G.; Zou, B. *J. Phys. Chem. B* **2011**, *115*, 8981.
(19) Li, S.; Li, Q.; Zhou, J.; Wang, R.; Jiang, Z.; Wang, K.; Xu, D.; Liu, J.; Liu, B.; Zou, G.; Zou, B. *J. Phys. Chem. B* **2012**, *116*, 3092.
(20) Wang, K.; Duan, D.; Wang, R.; Liu, D.; Tang, L.; Cui, T.; Liu, B.; Cui, Q.; Liu, J.; Zou, B.; Zou, G. *J. Phys. Chem. B* **2009**, *113*, 14719.
(21) Moggach, S.; Parsons, S.; Wood, P. *Crystallogr. Rev.* **2008**, *14*, 143.
(22) Boldyreva, E.; Ahsbahs, H.; Uchtmann, H.; Kashcheeva, N. *High Pressure Res.* **2000**, *17*, 79.
(23) Allan, D.; Clark, S.; Dawson, A.; McGregor, P.; Parsons, S. *Acta Crystallogr. B* **2002**, *58*, 1018.
(24) Boldyreva, E.; Shakhtshneider, T.; Ahsbahs, H.; Sowa, H.; Uchtmann, H. *Therm. Anal. Calorim.* **2002**, *68*, 437.
(25) Murli, C.; Sharma, S.; Karmakar, S.; Sikka, S. *Physica B: Condens. Matter* **2003**, *339*, 23.
(26) Dawson, A.; Allan, D.; Belmonte, S.; Clark, S.; David, W.; McGregor, P.; Parsons, S.; Pulham, C.; Sawyer, L. *Cryst. Growth Des.* **2005**, *5*, 1415.
(27) Goryainov, S.; Kolesnik, E.; Boldyreva, E. *Physica B: Condens. Matter* **2005**, *357*, 340.
(28) Goryainov, S.; Boldyreva, E.; Kolesnik, E. *Chem. Phys. Lett.* **2006**, *419*, 496.
(29) Dessen, A.; Quemard, A.; Blanchard, J.; Jacobs, W., Jr.; Sacchettini, J. *Science* **1995**, *267*, 1638.
(30) Somoskovi, A.; Wade, M.; Sun, Z.; Zhang, Y. *J. Antimicrob. Chemother.* **2004**, *53*, 192.
(31) Becker, C.; Dressman, J.; Amidon, G.; Junginger, H.; Kopp, S.; Shah, V.; Stavchansky, S.; Barends, D. *J. Pharm. Sci.* **2008**, *97*, 3709.
(32) Takaki, Y.; Sasada, Y.; Watanabe, T. *Acta Crystallogr.* **1960**, *13*, 693.
(33) Tamur, C.; Sasada, Y.; Kuwano, H. *Acta Crystallogr.* **1961**, *14*, 693.

(34) Ro, G.; Sorum, H. *Acta Crystallogr., Sect. B: Struct. Crystallogr. Cryst. Chem.* **1972**, *28*, 1677.
(35) Ro, G.; Sorum, H. *Acta Crystallogr., Sect. BL Struct. Crystallogr. Cryst. Chem.* **1972**, *28*, 991.
(36) Castro, R.; Maria, T.; Evora, A.; Feiteira, J.; Silva, M.; Beja, A.; Canotilho, J.; Euse bio, M. E. S. *Cryst. Growth Des.* **2009**, *10*, 274.
(37) Cherukuvada, S.; Thakuria, R.; Nangia, A. *Cryst. Growth Des.* **2010**, *10*, 3931.
(38) Mao, H.; Bell, P.; Shaner, J.; Steinberg, D. *J. Appl. Phys.* **1978**, *49*, 3276.
(39) Hammersley, A.; Svensson, S.; Hanfland, M.; Fitch, A.; Hausermann, D. *High Pressure Res.* **1996**, *14*, 235.
(40) Chis, V.; Pirnau, A.; Jurca, T.; Vasilescu, M.; Simon, S.; Cozar, O.; David, L. *Chem. Phys.* **2005**, *316*, 153.
(41) Hamann, S.; Linton, M. *Aust. J. Chem.* **1976**, *29*, 1641.
(42) Murnaghan, F. *Proc. Natl. Acad. Sci. U. S. A.* **1944**, *30*, 244.
(43) Oswald, I.; Urquhart, A. *Cryst. Eng. Commun.* **2011**, *13*, 4503.
(44) Hamann, S.; Linton, M. *Aust. J. Chem.* **1976**, *29*, 1825.
(45) Deb, S.; Rekha, M.; Roy, A.; Vijayakumar, V.; Meenakshi, S.; Godwal, B. *Phys. Rev. B* **1993**, *47*, 11491.
(46) Rao, R.; Sakuntala, T.; Godwal, B. *Phys. Rev. B* **2002**, *65*, 054108.
(47) Dreger, A.; Gupta, M. *J. Phys. Chem. B* **2007**, *111* (15), 3893.